AIP | Applied Physics Letters

Band offsets of n-type electron-selective contacts on cuprous oxide (Cu2O) for photovoltaics

Riley E. Brandt, Matthew Young, Helen Hejin Park, Arrelaine Dameron, Danny Chua, Yun Seog Lee, Glenn Teeter, Roy G. Gordon, and Tonio Buonassisi

Citation: Applied Physics Letters **105**, 263901 (2014); doi: 10.1063/1.4905180
View online: http://dx.doi.org/10.1063/1.4905180
View Table of Contents: http://scitation.aip.org/content/aip/journal/apl/105/26?ver=pdfcov
Published by the AIP Publishing

Band offsets of *n*-type electron-selective contacts on cuprous oxide (Cu_2O) for photovoltaics

Riley E. Brandt,[1,a)] Matthew Young,[2] Helen Hejin Park,[3] Arrelaine Dameron,[2] Danny Chua,[3] Yun Seog Lee,[1,b)] Glenn Teeter,[2] Roy G. Gordon,[3] and Tonio Buonassisi[1,a)]
[1]*Massachusetts Institute of Technology, Cambridge, Massachusetts 02139, USA*
[2]*National Renewable Energy Laboratory, Golden, Colorado 80401, USA*
[3]*Harvard University, Cambridge, Massachusetts 02139, USA*

(Received 23 October 2014; accepted 15 December 2014; published online 29 December 2014)

The development of cuprous oxide (Cu_2O) photovoltaics (PVs) is limited by low device open-circuit voltages. A strong contributing factor to this underperformance is the conduction-band offset between Cu_2O and its *n*-type heterojunction partner or electron-selective contact. In the present work, a broad range of possible *n*-type materials is surveyed, including ZnO, ZnS, Zn(O,S), (Mg,Zn)O, TiO_2, CdS, and Ga_2O_3. Band offsets are determined through X-ray photoelectron spectroscopy and optical bandgap measurements. A majority of these materials is identified as having a negative conduction-band offset with respect to Cu_2O; the detrimental impact of this on open-circuit voltage (V_{OC}) is evaluated through 1-D device simulation. These results suggest that doping density of the *n*-type material is important as well, and that a poorly optimized heterojunction can easily mask changes in bulk minority carrier lifetime. Promising heterojunction candidates identified here include Zn(O,S) with [S]/[Zn] ratios >70%, and Ga_2O_3, which both demonstrate slightly positive conduction-band offsets and high V_{OC} potential. This experimental protocol and modeling may be generalized to evaluate the efficiency potential of candidate heterojunction partners for other PV absorbers, and the materials identified herein may be promising for other absorbers with low electron affinities. © *2014 AIP Publishing LLC*. [http://dx.doi.org/10.1063/1.4905180]

Cuprous oxide (Cu_2O) is a promising Earth-abundant photovoltaic (PV) absorber, however, its technological relevance is limited by low PV conversion efficiencies.[1] In particular, historical cells demonstrate low open-circuit voltages (V_{OC}) relative to their Shockley-Queisser entitlement of 1.6 V. While low minority-carrier lifetime contributes to underperforming V_{OC}, recent work suggests that a dominant V_{OC} loss mechanism is the conduction-band alignment (offset) between Cu_2O and its heterojunction partner,[1–4] herein referred to as the electron-selective contact (ESC). Engineering this offset has led to open-circuit voltages as high as 1.2 V,[5] thus, we identify control, measurement, and modeling of the ESC conduction-band alignment as a critical area of research for Cu_2O. This method for screening the V_{OC} potential of candidate ESCs generalizes to other *p*-type absorber materials as well.

The search for more optimal ESCs is especially difficult due to the low electron affinity of Cu_2O ($\chi = 3.2$ eV); materials with such a low electron affinity are often challenging to dope *n*-type due to self-compensation by intrinsic defects.[6,7] Several authors have measured negative, or "cliff"-type conduction-band offsets between Cu_2O and other materials to explain the cause of low V_{OC}, including ZnO (−1.0 – −1.8 eV),[2,4,8,9] In_2O_3 (−0.83 eV),[10] TiO_2 (−0.74 eV),[11] GaN (−0.23 eV),[8] as well as ZnS and ZnSe.[12] In the present study, we specifically measure *n*-type materials deposited by atomic layer deposition (ALD) or pulsed laser deposition on electrochemically deposited Cu_2O terminated with a stoichiometric Cu_2O surface. The ESC materials explored include Zn(O,S), TiO_2, Ga_2O_3, CdS, and (Mg,Zn)O:Ga.

Electronic band offsets are sensitive to grain orientation,[13] surface atomic termination, adsorbed extrinsic species, chemical reactions, and interdiffusion.[14] Prior work suggests that the offset on Cu_2O is influenced by the presence of monolayers of CuO at the surface, which may explain the variation in literature reports of band offsets.[4] To control for these effects, all Cu_2O surfaces here are (111) terminated and show only the +1 oxidation state of copper as measured by X-ray photoelectron and Auger electron spectroscopy.

Cu_2O is deposited by constant-current two-electrode electrochemical deposition from a basic solution of copper sulfate, lactic acid, and sodium hydroxide. The deposition parameters are described in prior work.[2] A bath pH of 12.5 leads to the highly preferential (111) surface orientation. The film is rinsed in DI water (18.6 MΩ), and stored and transferred in a N_2 ambient glovebox to prevent surface oxidation to CuO. Unless stated otherwise, all depositions onto the Cu_2O are performed with a substrate temperature of 120 °C.

ZnO_xS_y and Ga_2O_3 overlayers are deposited by ALD with a custom tube furnace ALD reactor. Diethylzinc[15] and bis(μ-dimethylamino)tetrakis(dimethylamino)digallium[5] are used for the Zn and Ga precursors, respectively; deionized H_2O and 4% H_2S in N_2 are used for the oxide and sulfide anion precursors.

ZnO, CdS, and TiO_2 overlayers are deposited by ALD using a Beneq TFS200 ALD reactor. The cation precursors used are diethylzinc, dimethylcadmium, and titanium isopropoxide, respectively, while the anion precursors are the

a)Authors to whom correspondence should be addressed. Electronic addresses: rbrandt@alum.mit.edu and buonassisi@mit.edu
b)Present address: IBM T.J. Watson Research Center, Yorktown Heights, New York 10598, USA.

same as above. Deposition temperatures were again 120 °C except for TiO_2 deposited at 150 °C.

A gallium-doped magnesium zinc oxide alloy, (Mg,Zn)O:Ga, is deposited by pulsed laser deposition using two fixed-composition ceramic targets with 21% Mg or 6% Mg and 1% Ga; the deposition tool is described elsewhere.[16] Depositions were conducted at a chamber pressure of 9 mTorr, with a 99% Ar and 1% O_2 gas environment.

The valence- and conduction-band offsets are measured through a combination of X-ray photoelectron spectroscopy (XPS), UV-visible spectrophotometry, and spectroscopic ellipsometry. XPS is performed with a Kratos AXIS Nova tool, with a photon energy of 1486.6 eV. Samples experienced <10 min of ambient air exposure during mounting, then were pumped down to pressures $<10^{-8}$ mTorr for measurements. The binding energy scale is calibrated in each run by a linear least squares fitting of reference core levels of Cu 2*p*, Ag 3*d*, Mo 3*d*, and Au 4*f*, as well as Fermi levels of all four metals.

The valence band offset (ΔE_V) is determined by the Kraut method through XPS,[17] using core-level offsets from heterojunction samples

$$\Delta E_V = (E_V^{Cu_2O} - E_V^n) = (E_{core}^{Cu_2O} - E_{core}^n) - (E_{core}^{Cu_2O} - E_V^{Cu_2O}) + (E_{core}^n - E_V^n), \quad (1)$$

where E_V is the valence band maximum of Cu_2O or the *n*-type material and E_{core} is a specific core level for the Cu_2O or *n*-type material. Three samples are requisite—two bulk, homogeneous films to determine the core level to valence band offsets, and one heterojunction film with a thin overlayer on Cu_2O to determine the core level offsets. ALD ensures conformal overlayer coverage even at these thicknesses. The extraction of all three terms in Eq. (1) is demonstrated in Fig. 1 for ZnS on Cu_2O, where E_F is the Fermi energy, E_C is the conduction-band energy, and E_G represents the respective bandgaps.

To extract the conduction-band offset, ΔE_C, we add the difference in bandgap of the Cu_2O and ESC materials to ΔE_V. E_G is determined by fitting the absorption coefficient, measured through UV-visible spectrophotometry or spectroscopic ellipsometry. This necessarily assumes that the optical bandgap is identical to the fundamental bandgap (no Moss-Burstein shift), and that the surface bandgap is the same as the bulk bandgap.

The *n*-type materials in this study are amorphous with the exception of (Mg,Zn)O, pure ZnO, CdS, and pure ZnS as verified by X-ray diffraction (XRD). For amorphous materials, the band edge is fit by the Tauc method,[18] extrapolating the linear region of E_{photon} vs. $(\alpha h\nu)^{1/2}$, and for crystalline materials using the plot of E_{photon} vs. $(\alpha h\nu)^2$ instead.[19] The bandgap of Ga_2O_3 was determined previously to be 5.18 eV.[5]

For each material evaluated, the valence band offset is determined using the core level offset for an overlayer <2 nm thick. Given a carrier concentration in the overlayer of less than 1×10^{18} cm^{-3}, this results in a maximum electric field at the heterojunction of less than 5×10^4 V/cm. This corresponds to a shift in the binding energies of <0.01 eV over a 2 nm distance; thus, we assume that the effect of band bending is minimal over the typical XPS information depth.

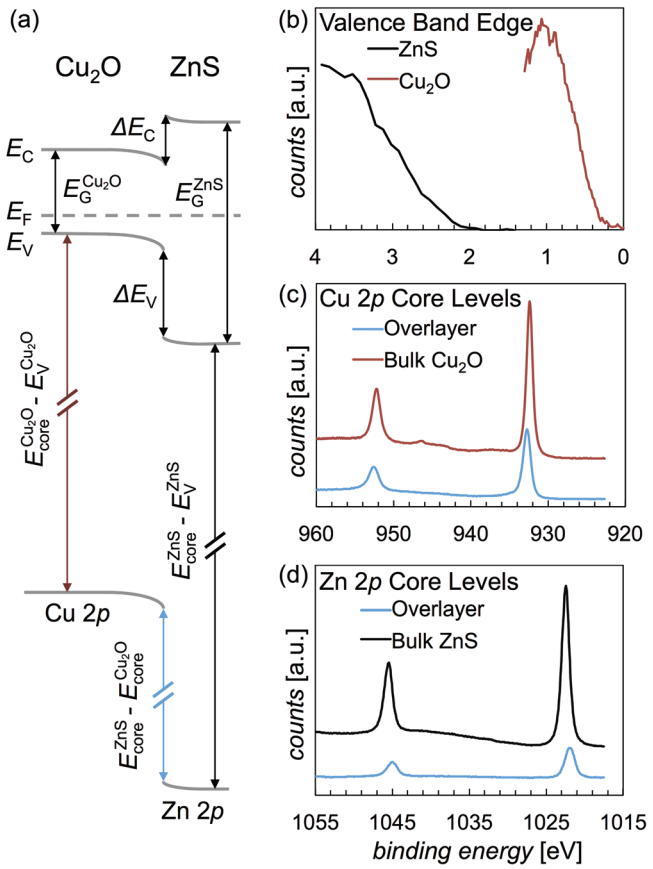

FIG. 1. Routine for ΔE_V extraction using 2 nm ZnS overlayers, with three samples; (a) band diagram of heterojunction with core-level to valence bands of separate bulk samples, and core-level offset; (b) valence band edges of pure, bulk samples; (c) Cu 2*p* core levels of pure bulk Cu_2O and with a thin overlayer; (d) Zn 2*p* core levels of pure bulk ZnS and in a thin overlayer sample.

The results of the core level to valence band and core level to Cu 2*p* 3/2 core level offsets are catalogued in Table I for each *n*-type material.

A 95% confidence interval for all valence-band offset measurements is determined to be ±0.10 eV by measuring eight identical Cu_2O samples.[19] Error bars for the bandgap are determined from selecting different fitting regions and computing the standard error of the least-squares fit line. The error bars in the conduction-band offsets are assumed to be the sum of the bandgap and valence band offset errors. All of the offsets measured here are plotted in Fig. 2.

To determine an optimal conduction-band offset, we simulate the effect of ΔE_C on V_{OC} and solar cell efficiency. The V_{OC} is determined by the hole and electron electrochemical potential difference, or quasi-Fermi level separation in the material. This separation may be limited by bulk recombination, which reduces the concentration of free photoexcited carriers, or limited by the electrochemical potential of electrons in the *n*-type ESC.[21] At the heterojunction interface, the recombination current, $J_{0,IF}$, may be modeled as

$$J_{0,IF} = S_h N_V e^{\frac{-q\varphi_{b0}}{k_B T}}, \quad (2)$$

where S_h is the hole surface recombination velocity (SRV) at the heterojunction and is proportional to interface defect density and capture cross-section, N_V is the valence band density

TABLE I. Extracted parameters for each *n*-type material from XPS and optical bandgap measurements, and the resulting band offsets including error estimates for bandgap E_G, ΔE_V, and ΔE_C. Cu_2O (Ref. 20) and Ga_2O_3 (Ref. 5) bandgaps taken from prior work.

Material	Core level	$E_{core} - E_V$ (eV)	$E_{core} - E_{Cu2p}$ (eV)	$E_V - E_F$ (eV)	E_G (eV)	ΔE_V (eV)	ΔE_C (eV)
Cu_2O	Cu 2*p* 3/2	931.97	…	0.35	2.09	…	…
ZnO	Zn 2*p* 3/2	1018.76	89.30	3.42	3.26 ± 0.01	−2.51 ± 0.10	−1.34 ± 0.11
$Mg_{0.06}Zn_{0.93}O$	Zn 2*p* 3/2	1018.75	89.55	3.72	3.71 ± 0.05	−2.77 ± 0.10	−1.15 ± 0.15
$Mg_{0.21}Zn_{0.78}O$	Zn 2*p* 3/2	1018.62	89.47	4.03	3.94 ± 0.02	−2.82 ± 0.10	−0.97 ± 0.12
$ZnO_{0.99}S_{0.09}$	Zn 2*p* 3/2	1019.12	89.14	2.98	3.02 ± 0.02	−1.99 ± 0.10	−1.06 ± 0.12
$ZnO_{0.82}S_{0.26}$	Zn 2*p* 3/2	1019.87	89.25	2.28	2.60 ± 0.05	−1.35 ± 0.10	−0.84 ± 0.15
$ZnO_{0.64}S_{0.50}$	Zn 2*p* 3/2	1020.08	89.27	2.20	2.76 ± 0.04	−1.16 ± 0.10	−0.49 ± 0.14
$ZnO_{0.50}S_{0.64}$	Zn 2*p* 3/2	1020.20	89.22	2.38	2.96 ± 0.04	−0.99 ± 0.10	−0.12 ± 0.14
$ZnO_{0.42}S_{0.73}$	Zn 2*p* 3/2	1020.25	89.18	2.27	2.93 ± 0.02	−0.90 ± 0.10	−0.06 ± 0.12
ZnS	Zn 2*p* 3/2	1020.20	89.18	2.27	3.67 ± 0.01	−0.95 ± 0.10	0.63 ± 0.11
TiO_2	Ti 2*p* 3/2	455.63	−473.78	3.72	3.44 ± 0.01	−2.56 ± 0.10	−1.21 ± 0.11
CdS	Cd 3*d* 5/2	403.48	−527.52	2.64	2.38 ± 0.02	−0.97 ± 0.10	−0.68 ± 0.12
Ga_2O_3	Ga 2*p* 3/2	1114.91	185.65	4.21	5.18 ± 0.02	−2.71 ± 0.10	0.38 ± 0.12

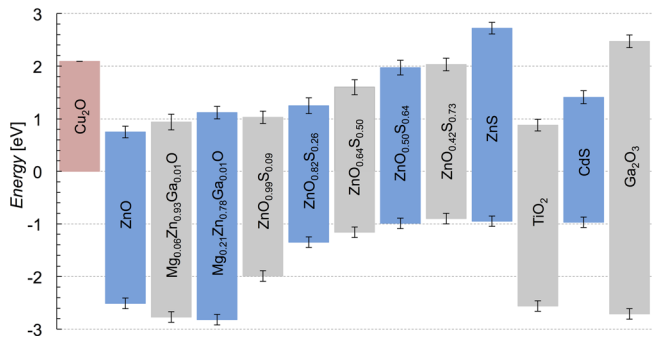

FIG. 2. Band energies (in flat-band condition) of *n*-type materials with respect to Cu_2O and their respective error bars. All energies are referenced to the valence band of Cu_2O.

of states in Cu_2O, φ_{b0} is the potential barrier for holes at the heterojunction (see Fig. 3(a)), q is the charge of an electron, and k_BT is the product of the Boltzmann constant and temperature.[22] If this recombination current is the dominant recombination mechanism, the V_{OC} is limited to a maximum of φ_{b0}, which is determined by the conduction-band offset and donor/acceptor density N_D/N_A ratio between the ESC and Cu_2O. Thus, we would expect the V_{OC} to improve with increasing donor density in the buffer (N_D), a less cliff-like conduction-band offset, and decreasing SRV.

We quantify this with a SCAPS-1D device model of a heterojunction thin-film Cu_2O device. Here, the Cu_2O is assumed to have a $1\,cm^2\,V^{-1}\,s^{-1}$ minority carrier mobility, typical of electrochemically deposited Cu_2O.[23] The Cu_2O and *n*-type partners are modeled with bandgaps of 2.09 eV (Ref. 20) and 3.3 eV, as well as carrier concentrations of $10^{15}\,cm^{-3}$ and 10^{16}–$10^{19}\,cm^{-3}$, respectively. Changing the concentration of neutral, mid-gap interface defects influences the interface recombination velocity, while changing the concentration of neutral mid-gap bulk defects influences the bulk lifetime. As expected, the V_{OC} decreases with increasing SRV, and drops linearly with decreasing conduction-band offset and logarithmically with decreasing ESC donor density (Fig. 3(c)) for cliff-type offsets. A thousand-fold increase in bulk lifetime results in minimal change in V_{OC} over this region.

For near-zero ΔE_C, the V_{OC} becomes bulk-recombination dominated instead, and is determined by bulk lifetime alone, making it insensitive to changes in ΔE_C and SRV (Fig. 3(b)), as well as ESC donor density (Fig 3(c)). The transition between these bulk-recombination and interface-recombination limits occurs at different offsets depending upon the SRV and ESC doping density. In the extreme case of a defect-free interface (low SRV) and low-lifetime bulk material, a slight cliff can moderately improve the V_{OC} by providing a barrier for electrons in the ESC from diffusing back into the low-lifetime bulk Cu_2O and recombining with holes. This effect disappears at higher SRVs.

The importance of simultaneous optimization of the band alignment, reduction in defect density, and maximization of ESC doping density is exemplified by the case of silicon heterojunction with intrinsic thin layer (HIT) cells,[24] which enables these heterojunction solar cells to exhibit higher V_{OC} than homojunction cells by reducing emitter and interface recombination.

Based on these simulation results, for many conventional *n*-type electron-selective contacts or buffer layers, the

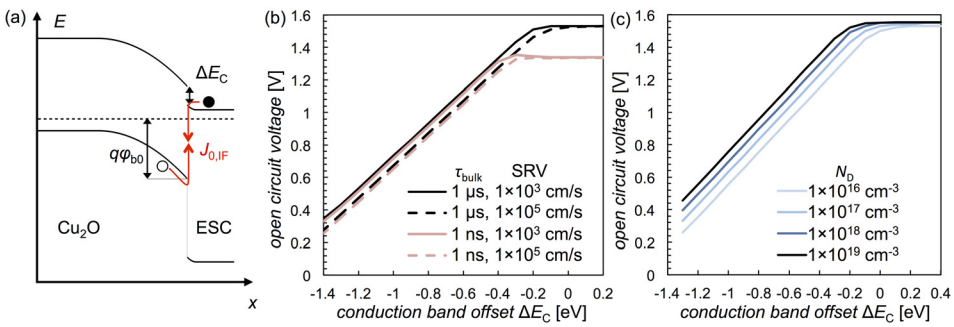

FIG. 3. (a) Band diagram of cliff-type offset showing the barrier height and pathway for interface recombination; (b) and (c) V_{OC} entitlement plotted as a function of conduction-band offset for a simple Cu_2O/*n*-type semiconductor heterojunction, varying the bulk lifetime and SRV in (b) and varying the ESC donor density in (c).

band alignment on Cu_2O is not favorable for fabricating a high-quality heterojunction. This is demonstrated by the large conduction-band cliff measured for ZnO, TiO_2, and CdS.

However, alloying in the ZnO system demonstrates the potential for improving conduction-band alignment, especially when S assumes fractional occupancy on the anion site.[25] Significant bandgap bowing necessitates going to high sulfur contents to achieve good alignment. While pure ZnS demonstrates a prohibitively large spike, intermediate compositions with a [S]/[Zn] ratio >70% show near-ideal alignment (note here that the ALD Zn(O,S) has a total anion/cation ratio greater than one due to extra hydroxide and oxide incorporation). Attempts to increase the ZnO conduction band via cation substitution are only marginally successful; this explains why alloying with Mg or Sn on the Zn site has been insufficient to make a high-performance heterojunction.[2,3]

Another promising material is Ga_2O_3, which offers near ideal electronic alignment. This alignment has led to the record-high open circuit voltages in thermally oxidized (0.8 V)[26] and electrochemically deposited (1.2 V)[5] Cu_2O cells. The offset measured in the present study represents an increase over the previous measurement of -0.18 ± 0.16 eV,[5] which is likely due to differences in surface preparation or deposition conditions. This highlights the necessity of direct measurements under device-relevant conditions.

To address interface defect density and SRV, we limit the formation of detrimental surface phases during storage and processing. All bare Cu_2O surfaces show no evidence of CuO phase, which has been identified as a detrimental defect at Cu_2O heterojunctions.[4,27] For sulfides used here, we note that exposure of a clean Cu_2O surface to the H_2S sulfur precursor, under typical ALD conditions, resulted in the formation of Cu-S bonds at the surface as evidenced by the presence of S core peaks in XPS. However, it is unclear whether Cu-S bonds form at the interface during sulfide deposition. This is because it is difficult to distinguish between Cu_2S and Cu_2O at a buried interface using XPS, given their nearly identical core electron binding energies.

In summary, one promising strategy to improve conduction-band alignment with Cu_2O's low electron affinity involves creating ternary alloys from conventional ESC materials. Alloying on the anion site with larger isovalent elements pushes the valence-band and conduction-band orbitals up to higher energies. This is demonstrated here with Zn(O,S), which shows an ideal conduction-band offset for sulfur contents >70%. Similar improvements alloying with Mg on the cation site are limited by the poor miscibility of (Mg,Zn)O at higher Mg content. The success of this ternary approach also suggests that intermediate compositions of (Zn,Cd)S would also have optimal alignment.

A second approach is to seek unconventional *n*-type buffer layers that may have reduced conductivity, but an innately lower electron affinity. Ga_2O_3 is demonstrated here as a promising candidate, which explains its role in the highest performing literature devices to date. However, the simulation results suggest that higher carrier concentration is necessary for high-performing devices, thus, extrinsic doping of Ga_2O_3 (e.g., Sn, Ge, F), and Zn(O,S) (e.g., Al, Ga, F) are high-priority areas of research.

Other emerging PV absorber materials including SnS or Zn_3P_2 exhibit similarly low electron affinities as Cu_2O. The present work points to the challenges in pairing these absorbers with conventional *n*-type buffer layers. However, it also points to the value of developing ternary, tunable buffer layers, and unconventional materials that may greatly expand the range of commercially viable PV materials in the future.

This work was supported by an NSF CAREER Award ECCS-1150878, the National Research Foundation Singapore through the Singapore Massachusetts Institute of Technology Alliance for Research and Technology's Low Energy Electronic Systems research program, and the National Renewable Energy Laboratory as a part of the Non-Proprietary Partnering Program under Contract No. DE-AC36-08-GO28308 with the U.S. Department of Energy. This work made use of the Center for Nanoscale Systems at Harvard University supported by NSF Award ECS-0335765. An NSF Graduate Research Fellowship (R.E.B.) is acknowledged. R.E.B. acknowledges helpful conversations with Dr. R. Jaramillo and Dr. N. M. Mangan.

R.E.B. designed the experiment, fabricated Cu_2O and PLD samples, and wrote the paper; M.Y. took XPS measurements; R.E.B., M.Y., and G.T. analyzed the data; H.H.P., A.D., and D.C. deposited ALD films and took optical data; Y.S.L., R.G.G., and T.B. advised in experimental planning, reviewed data analysis, and assisted in manuscript preparation.

[1]B. K. Meyer, A. Polity, D. Reppin, M. Becker, P. Hering, P. J. Klar, T. Sander, C. Reindl, J. Benz, M. Eickhoff, C. Heiliger, M. Heinemann, J. Bläsing, A. Krost, S. Shokovets, C. Müller, and C. Ronning, Phys. Status Solidi B **249**, 1487 (2012).
[2]Y. S. Lee, J. Heo, S. C. Siah, J. P. Mailoa, R. E. Brandt, S. B. Kim, R. G. Gordon, and T. Buonassisi, Energy Environ. Sci. **6**, 2112 (2013).
[3]Z. Duan, A. Du Pasquier, Y. Lu, Y. Xu, and E. Garfunkel, Sol. Energy Mater. Sol. Cells **96**, 292 (2012).
[4]S. S. Wilson, J. P. Bosco, Y. Tolstova, D. O. Scanlon, G. W. Watson, and H. A. Atwater, Energy Environ. Sci. **7**, 3606 (2014).
[5]Y. S. Lee, D. Chua, R. E. Brandt, S. C. Siah, J. V. Li, J. P. Mailoa, S. W. Lee, R. G. Gordon, and T. Buonassisi, Adv. Mater. **26**, 4704 (2014).
[6]S. B. Zhang, J. Phys. Condens. Matter **14**, R881 (2002).
[7]W. Walukiewicz, Phys. B Condens. Matter **302**, 123 (2001).
[8]B. Kramm, A. Laufer, D. Reppin, A. Kronenberger, P. Hering, A. Polity, and B. K. Meyer, Appl. Phys. Lett. **100**, 094102 (2012).
[9]D. Zhang, Y. Liu, Y. Liu, and H. Yang, Phys. B Condens. Matter **351**, 178 (2004).
[10]C. J. Dong, W. X. Yu, M. Xu, J. J. Cao, C. Chen, W. W. Yu, and Y. D. Wang, J. Appl. Phys. **110**, 073712 (2011).
[11]L. Huang, F. Peng, and F. S. Ohuchi, Surf. Sci. **603**, 2825 (2009).
[12]S. S. Wilson, J. P. Bosco, Y. Tolstova, and H. A. Atwater, *2013 MRS Fall Meet.* (Boston, MA, 2013), p. Z7.01.
[13]V. Stevanović, K. Hartman, R. Jaramillo, S. Ramanathan, T. Buonassisi, and P. Graf, Appl. Phys. Lett. **104**, 211603 (2014).
[14]L. Chkoda, C. Heske, M. Sokolowski, E. Umbach, F. Steuber, J. Staudigel, M. Stößel, and J. Simmerer, Synth. Met. **111–112**, 315 (2000).
[15]H. Hejin Park, R. Heasley, and R. G. Gordon, Appl. Phys. Lett. **102**, 132110 (2013).
[16]Y. Ke, J. Berry, P. Parilla, A. Zakutayev, R. O'Hayre, and D. Ginley, Thin Solid Films **520**, 3697 (2012).
[17]E. A. Kraut, R. W. Grant, J. R. Waldrop, and S. P. Kowalczyk, Phys. Rev. Lett. **44**, 1620 (1980).
[18]J. Tauc, R. Grigorovici, and A. Vancu, Phys. Status Solidi **15**, 627 (1966).
[19]See supplementary material at http://dx.doi.org/10.1063/1.4905180 for determination of bandgaps from Tauc plots, and quantification of error bars.
[20]C. Malerba, F. Biccari, C. Leonor Azanza Ricardo, M. D'Incau, P. Scardi, and A. Mittiga, Sol. Energy Mater. Sol. Cells **95**, 2848 (2011).

[21]T. Minemoto, T. Matsui, H. Takakura, Y. Hamakawa, T. Negami, Y. Hashimoto, T. Uenoyama, and M. Kitagawa, Sol. Energy Mater. Sol. Cells **67**, 83 (2001).
[22]J. V. Li, S. Grover, M. A. Contreras, and R. Noufi, Sol. Energy Mater. Sol. Cells **124**, 143 (2014).
[23]K. Mizuno, M. Izaki, K. Murase, T. Shinagawa, M. Chigane, M. Inaba, A. Tasaka, and Y. Awakura, J. Electrochem. Soc. **152**, C179 (2005).
[24]M. Taguchi, A. Terakawa, E. Maruyama, and M. Tanaka, Prog. Photovoltaics: Res. Appl. **13**, 481 (2005).
[25]C. Persson, C. Platzer-Björkman, J. Malmström, T. Törndahl, and M. Edoff, Phys. Rev. Lett. **97**, 146403 (2006).
[26]T. Minami, Y. Nishi, and T. Miyata, Appl. Phys. Express **6**, 044101 (2013).
[27]S. W. Lee, Y. S. Lee, J. Heo, S. C. Siah, D. Chua, R. E. Brandt, S. B. Kim, J. P. Mailoa, T. Buonassisi, and R. G. Gordon, Adv. Energy Mater. **4**, 1301916 (2014).